Wind-fed X-ray binaries:
Collision of gas streams near a rotating black hole

Sara Bergenius

April 29, 2000

Abstract

In a binary system where the two companions are a massive OB-star and a black hole, matter is transferred through the wind of the OB-star. A small part of the material will be captured by the gravitational field of the black hole. The specific angular momentum of the captured matter is modest, comparable to $\sim r_g c$, where r_g is the Schwarzschild radius of the black hole. At large distances, $r \gg r_g$, matter is in spherical free-fall. At $r \sim r_g$ the angular momentum becomes dynamically important, leading to collision of gas streams near the black hole. In this thesis, I will study how the rotation of the black hole affects the collision radius, and calculate the minimum angular momentum the matter should have to collide outside the black hole horizon.

Contents

1 Introduction

I thought a long time about how I should begin this thesis. It had to be something that would catch the reader's interest, maybe something philosophical that would make all the everyday problems seem insignificant. But I just could not think of anything to write. Instead an old memory came back to me, a memory from the time when I was about five years old. I had just learned how to count to twenty, a very large number at that time. The largest number I had ever heard of was a hundred, and I remembered thinking that if twenty was the largest number I could count to, and hundred was the largest number existing, twenty plus twenty must be a hundred. I could not help smiling at this memory, and think about how I would look upon the world had I not attended school and learned that twenty plus twenty was forty and nothing else. I wonder what this thesis would have looked like if I had kept that logic. Well, eventually I did attend school, and this is what the thesis came to look like, and now when I got you to read this far, you might as well read the rest.

It all began during the 1960s, when astrophysicists discovered sources of X-rays scattered across the sky. These sources was later recognized as *X-ray binaries*, and they constitute the foundation of which this thesis lies upon. I will start by explaining what an X-ray binary is, and since we will be dealing with a black hole as one of the components in the binary, I will also give a brief introduction to black holes, and that will be extended to a more mathematical description further on. In section 2 and 3 the problem is described in more detail. Wind-fed accretion is reviewed, first on a large scale, and then on a small scale. In section 5, we study the trajectories of streamlines in the gravitational field of a rotating black hole. The results and the conclusions are given in section 6.

1.1 X-ray binaries

Almost half of all the stars we can see (in our vicinity) are in fact part of a binary system. The existence of the X-ray binaries was discovered by rocket flights in the 1960s, and at that time no known physical process was capable of generating the enormous X-ray luminosities found. In the mid-1960s came the optical identification of Sco X-1 and Cyg X-2, two radio sources, and it was remarkable how visually faint (13th to 15th magnitude) these extremely powerful X-ray sources were. The absence of absorption features, as in the normal (solar type) spectrum, indicated that little or none of the light observed was coming from a main sequence star. There was a great deal of theoretical speculation about the nature of the energy source in Sco X-1 and this centered around white dwarfs, neutron stars and black holes. At that time these were very exotic objects - pulsars had yet not been discovered and neutron stars existed only in the minds of theoreticians.

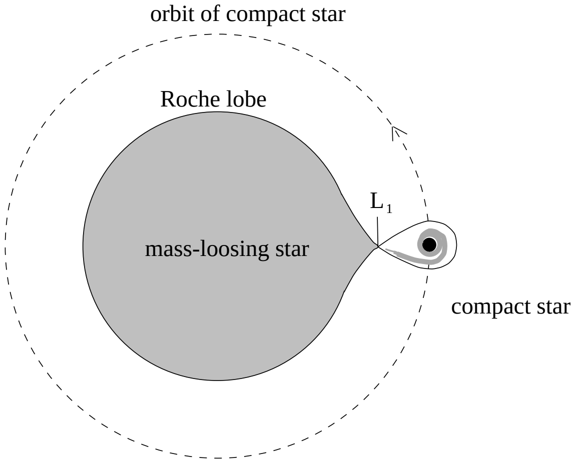

Figure 1: Schematic picture of low-mass X-ray binary system. The mass-losing star has expanded and overflows its Roche lobe. The gas flows through the inner Lagrange point, L_1, and and accretes onto the compact object through an accretion disc.

The presence of ionized helium indicated that the source of excitation of the lines was very hot and very likely to be connected with X-rays.

In 1970 UHURU (or SAS-1, Small Astronomy Satellite-1) made the first comprehensive survey of the X-ray sky, and it found two sources which were pulsating regularly with extremely precise periods. They both showed X-ray eclipses and it was recognized immediately that they both were close binary systems in which the X-ray emitting object was a rapidly spinning neutron star. It could not be a white dwarf since it would break up due to centrifugal forces if spinning with such a short period. Matter was transferred from one component onto the compact object, thereby releasing a large amount of gravitational energy in the form of X-rays.

It was quickly realized that there were two basic forms that systems with a neutron star or a black hole could take, and in which mass could be transferred from one star onto the other:

***Class I*:** Massive X-Ray Binaries (MXRBs)
In these binaries the material for transfer is provided by a powerful stellar wind from an early-type, massive OB star. The wind is so powerful that sufficient material is being lost in all directions for the compact object to accrete and produce copious X-rays as it ploughs through this wind, thereby creating a comet shaped shock front. Cen X-3 and Cyg X-1 are both of this class.

***Class II*:** Low-Mass X-Ray Binaries (LMXBs)
If the mass-losing star is of low mass then it will not have a strong

stellar wind and hence cannot power the X-ray source by the same mechanism as in Class I sources. In this case the companion star has evolved to fill its Roche lobe (surface of equal gravity), and the presence of the compact object distorts the mass-losing star into a pear-like shape (see figure 1). Matter that overflows the Roche lobe forms a stream and accretes onto the compact object creating a disc. The transferred matter has a large angular momentum compared to the wind in the MXRBs, hence the disc formed in LMXBs will be larger. By viscous forces the matter is gradually accreted onto the compact object where the X-rays are generated. Sco X-1 and Her X-1 are Class II sources.

There is a great variety of objects and behavior patterns. Basically, many of the properties of a binary depends on the nature of the compact object.

1.2 Black holes

When a star has used up all its fuel, the core cannot support the pressure of the outer layers and the star collapses. If the star is massive, nothing can halt the collapse, and as the collapse proceeds, the gravitational field close to the star becomes stronger and stronger and eventually nothing, not even light, can escape from the object to the outside world. A black hole has been born. A black hole is defined simply as a region of space-time that cannot communicate with the external universe. The boundary of this region is called the surface of the black hole or the *event horizon*.

In 1795 Laplace noted that light could not escape from an object of sufficiently large mass and small radius. This was a consequence of Newtonian gravity and Newton's theory of light as particles. Nobody paid much attention to this new idea and it fell into oblivion for many years. Then in December 1915, within a month of the publication of Einstein's theory of general relativity, Karl Schwarzschild derived his relativistic solution for the gravitational field surrounding a spherical mass. He sent his paper to Einstein, who wrote back: "I had not expected that the exact solution to the problem could be formulated. Your analytical treatment to the problem appears to me splendid." This solution was the complete description of the external field of a spherical, electrically neutral, nonrotating black hole, and today we refer to such black holes as *Schwarzschild black holes*.

In 1930 Chandrasekhar discovered the existence of an upper limit to the mass of a cold, dense star, a so-called white dwarf, where the pressure of degenerate electrons prevent a gravitational collapse. This discovery implied that the inevitable fate of a sufficiently massive star must be the formation of a black hole. Still, physicists like Eddington and Landau would not accept this upper limit and the existence of black holes, even Einstein claimed that stars could not collapse to a single point.

In 1939, Oppenheimer and Volkoff calculated the upper mass limit for a neutron star, a star more compact than the white dwarf, and where the pressure is sustained by neutrons. In the same year the first rigorous calculation demonstrating the formation of a black hole was done by Oppenheimer and Snyder. With their calculation of the collapse of a homogeneous sphere of pressureless gas in general relativity, they found that the sphere eventually becomes cut off from all communication with the rest of the universe. However, black holes and the problem of gravitational collapse were again generally ignored until the 1960s, when Wheeler and his collaborates began a serious investigation of the problem of collapse. Wheeler coined the name "black hole" in 1968.

In 1963 R. Kerr found a set of solutions to Einstein's field equations which described rotating black holes, now referred to as *Kerr black holes.*

If one extrapolates Einstein's equations all the way inside a black hole, they break down and a singularity is developed. This singularity is hidden by the event horizon, it is causally disconnected from the outside world.

One might expect the solutions to Einstein's equations to be complicated, since black holes can be formed from stars with varying mass distributions, shapes, magnetic fields, angular momentum, and so on. But the most general stationary solution is known analytically and depends only on three parameters; the mass M, angular momentum, J, and charge Q of the black hole. All other information about the initial state is radiated away in form of electromagnetic and gravitational waves during the collapse. This was summarized by Wheeler as "A black hole has no hair".

It is difficult to prove that black holes really exist, the problem lies in detecting an object only a few kilometers across that emits no radiation itself. One way would be to find an X-ray binary system where one component is very compact. If one can find an X-ray binary in which the mass of the compact object exceeds $3M_\odot$, a strong case can be made that the compact object is a black hole. Observations of the binary X-ray source Cygnus X-1 in the early 1970s provided the first plausible evidence that black holes actually exist. Today there is a number of black hole candidates in our galaxy, and one also believes that active galactic nuclei (AGNs) are powered by accretion onto supermassive black holes.

2 Wind-fed accretion

In many X-ray binaries the mass-losing star does not fill its Roche lobe and the compact object accretes from the wind of the star. This is called wind-fed accretion and occurs in systems where the donor star is an OB-star. The massive OB-star produces a powerful stellar wind, which is approximately isotropic, i.e. the wind material leaves the surface uniformly in all directions. The wind velocity is high, $v_{\rm w} \sim 1-2\times 10^3$ km s^{-1}, and the star can have a

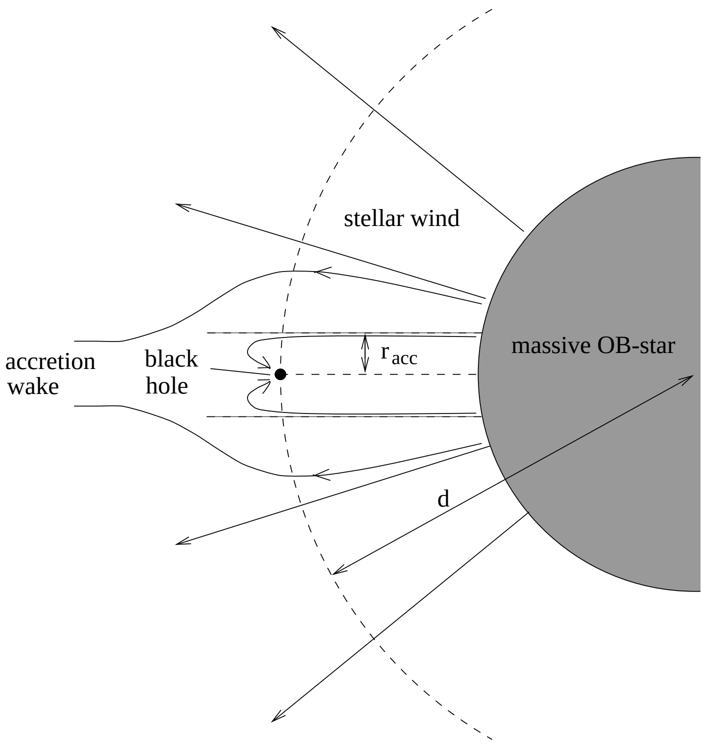

Figure 2: Wind-fed accretion from an OB-star onto a compact object. The gravitational field of compact object captures matter within the accretion cylinder.

mass loss up to $\dot{M} = 10^{-6} M_\odot \ \mathrm{yr}^{-1}$. We will be dealing with a binary system consisting of a massive OB-star and a black hole as its compact companion. The radius of the black hole is $r_g = 2GM/c^2$, the so-called Schwarzschild radius, where M is the mass of the black hole and c is the speed of light.

Only a small part of the wind will be captured by the gravitational field of the black hole. The captured wind forms an accretion cylinder, where material within a radius r_{acc} will be accreted, whereas material outside the cylinder will escape (see figure 2). This radius can be estimated by noting that material of mass m, will only be accreted if it has kinetic energy less than the potential energy in the gravitational field of the black hole

$$\frac{mv_{\mathrm{w}}^2}{2} \approx \frac{GMm}{r_{\mathrm{acc}}},$$

or, equivalently,

$$r_{\mathrm{acc}} \approx \frac{2GM}{v_{\mathrm{w}}^2}. \tag{1}$$

We can estimate r_{acc} by using that the wind velocity is approximately equal to the escape velocity from the donor surface which is $\approx 10^8$ cm/s for OB stars

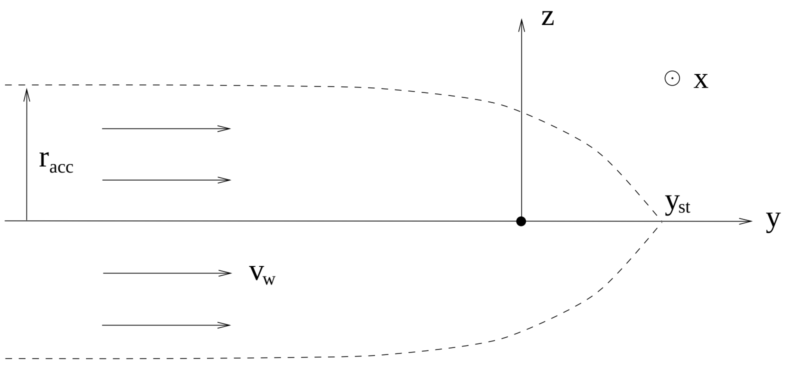

Figure 3: Axially symmetric flow in the free fall approximation (Bondi-Hoyle-Lyttleton model). The accretor is situated in the origin and the dashed lines represents the boundary of the accretion cylinder. $y_{\rm st}$ is the so-called stagnation point.

$$r_{\rm acc} \sim 3 \times 10^{10} \left(\frac{M}{M_\odot}\right) \left(\frac{v_{\rm w}}{10^8}\right)^{-2} \text{ cm.} \tag{2}$$

In these wind-fed binary systems, a typical value for $r_{\rm acc}$ is $\lesssim 10^{11}$ cm, and the separation between the objects is $d \sim 10^{12} - 10^{13}$ cm, so we can assume that the flow in the cylinder is plane-parallel before it reaches the accretor. To a first approximation we can also assume that the compact object is at rest relative to the wind, since the time it takes for the wind to reach the accretor, $d/v_{\rm w} \sim 10^4$ s, is much shorter than the orbital period $P \sim 10^6$ s. The flow is then nearly axisymmetric around the line connecting the two companions. In the axisymmetric approximation, the flow possesses no net angular momentum.

If the flow has no pressure, then the situation can be described by the so-called Bondi-Hoyle-Lyttleton model (Bondi & Hoyle 1944), in which the matter is assumed to be in free fall everywhere. Let us introduce a coordinate system (x, y, z), where the accretor is situated at the origin, the z-axis is perpendicular to the plane of the binary, and the y-axis is directed from the donor star to the accretor. The flow in the accretion cylinder is axisymmetric around the line connecting the two companions. Closer to the compact object, at $r \sim r_{\rm acc}$, the matter starts to get pulled by the gravitational field of the black hole (see figure 3). The deflected flow collides on the so-called "accretion line", $x = z = 0$, $y > 0$, and because of the symmetry, the x, z-components of the momentum cancel each other and we will only have motion in the y-direction. The boundary of the accretion cylinder transforms into a stagnation point, $y_{\rm st}$, and when $y < y_{\rm st}$ accretion occurs, while outside $y_{\rm st}$ gas flows out.

In reality, unlike the Bondi-Hoyle-Lyttleton model, the pressure becomes important at a distance $r \sim r_{\rm acc}$ from the compact object and the flow is

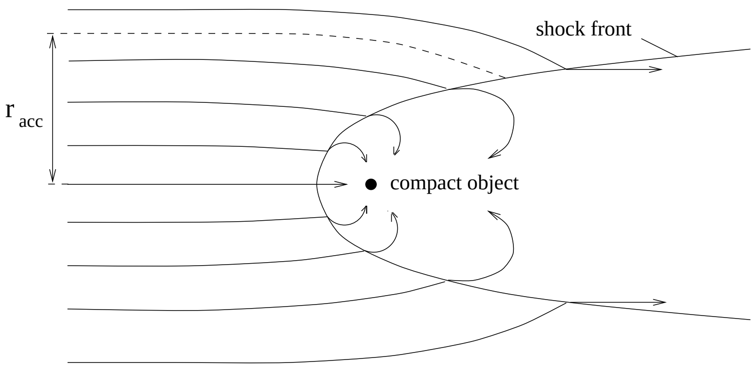

Figure 4: Streamlines of gas falls in supersonically towards the accretor. At $r \ll r_{\mathrm{acc}}$ a spherically symmetric inflow forms.

not in free fall anymore. The pressure increases as we get closer to the accretor, and if the wind from the donor star is supersonic then a bow shock arises. The flow before the shock is in free-fall, while behind the shock the flow becomes subsonic, i.e., the Mach number, $\mathcal{M} = v/c_s$, where $c_s = (10kT/3m_p)^{1/2}$ is the speed of sound and v is the velocity of the flow, is < 1. It was shown that at $r \ll r_{\mathrm{acc}}$ the flow forms a spherically symmetric inflow (Hunt 1971). So, at first, we have a plane-parallel flow which after the bow shock transforms into a three-dimensional, spherically symmetric inflow (see figure 4).

At approximately the same distance, $r \sim r_{\mathrm{acc}}$, the flow is also affected by Compton heating by the central source. This happens when the X-rays produced in the vicinity of the black hole heats the infalling matter by Compton scattering. It was shown by Illarionov & Kompaneets (1990) and Igumenshchev, Illarionov & Kompaneets (1993) that an inflow-outflow pattern of accretion forms under such conditions. Gas that becomes overheated by Compton scattering will reverse its motion because of increased pressure. Because of the anisotropy of the radiation from the accretion disc (the disc is more luminous face-on than edge-on), the infalling matter will experience more radiation along the poles than at the equator. Thus matter will flow out only at the poles while there is an inflow everywhere else. The inflow-outflow regime is established outside the so-called Compton radius,

$$r_{\mathrm{C}} = \frac{GMm_p}{5kT_{\mathrm{C}}} \approx 3 \times 10^9 \left(\frac{M}{M_\odot}\right) \left(\frac{T_{\mathrm{C}}}{10^8}\right)^{-1} \mathrm{cm}, \tag{3}$$

where T_{C} is the Compton temperature of the X-ray source. Inside this radius, an almost spherically symmetric inflow forms.

The Compton radius is typically $\sim 10^4 r_g \sim 10^{10}$ cm, about 10 times smaller than r_{acc}. Inside r_{C} the escape temperature T exceeds the Compton temperature T_C, and then the gas is Compton cooled by the X-rays rather than heated (The X-rays start to cool down the plasma efficiently as soon as the temperature exceeds T_C). As a result of Compton cooling, the speed of sound, c_s, is kept modest. The radial velocity of the flow increases and the Mach number exceeds unity, i.e. the inflow becomes supersonic. This means that at $r \ll r_C$, the gas is in free fall.

3 Formulation of the problem

Inside the Compton radius, the accreting matter is in nearly radial free-fall. The dynamics of the free-fall is determined by the boundary conditions at $r \sim r_C$. From the conservation of energy we have for parabolic infall

$$\frac{v^2}{2} \approx \frac{GM}{r} \qquad \Rightarrow \qquad v \approx \sqrt{\frac{2GM}{r}}.$$

When matter is in radial infall, $v_r \approx v$. The small nonradial component of the velocity, $v_\perp$, is determined by a (small) angular momentum per unit mass:

$$\begin{aligned} \mathbf{l} &= \mathbf{r} \times \mathbf{v}, \\ l &= r v_\perp \qquad \Rightarrow \qquad v_\perp = \frac{l}{r}. \end{aligned} \tag{4}$$

$v_\perp$ grows inward faster than v_r. As a result, v_r and $v_\perp$ can become comparable and a disc can form at the radius

$$r_d \sim \frac{l^2}{2GM} = \frac{l^2}{r_g c^2}. \tag{5}$$

The condition for disc formation around the black hole can be written as $r_d > r_g$, which reads $l > l_{\min}$, where $l_{\min} \sim r_g c$.

The expected angular momentum of a wind-fed accretion flow is small, however, it is not exactly zero because the binary is rotating. The resulting angular momentum was estimated theoretically by Illarionov & Sunyaev (1975) and Shapiro & Lightman (1976)

$$l = \frac{1}{4}\eta \Omega r_{\rm acc}^2, \tag{6}$$

where Ω is the angular velocity of the binary system and $\eta \sim 1$ is a numerical factor. With the accretion radius from equation (2) we get that

$$\frac{l}{r_g c} \approx 1.5 \eta P^{-1} \left(\frac{M}{M_\odot}\right) \left(\frac{v_{\rm w}}{10^8}\right)^{-4}, \tag{7}$$

where $P = 2\pi/\Omega$ is the binary period measured in days. The typical parameters of observed massive X-ray binaries, where one of the companions is a black hole, are $P \sim$ a few days, $M \sim 3 - 10M_\odot$ (Tanaka & Lewin 1995). Thus the typical captured angular momentum is rather small, of the order $r_g c$, and the accretion is radial almost all the way down to the black hole. However, in the very vicinity of the black hole, at $r \sim r_g$, a disc may form. The value of the angular momentum is just on the threshold for formation of a small-scale disc.

In the case where a small-scale disc is formed, the disc will be responsible for most of the emission. The gas that instead hits the event horizon of the black hole will have low radiative efficiency. This is so because the black hole does not possess a hard surface in the physical sense. The infalling matter will not "collide" with the surface of the black hole, instead it passes the event horizon and never comes back. (By contrast, in the case where the compact object is a neutron star, matter that collides with its surface is shocked and emits X-rays). When the compact object is a black hole, the accretion flow can produce a large luminosity only if its streamlines collide outside r_g. The formation of a small-scale disc is thus crucial: the black hole "switches on" as a luminous source when l exceeds $l_{\rm min}$ and the disc forms.

The picture of wind-fed accretion with $l \sim l_{\rm min}$ onto a Newtonian accretor was discussed by Illarionov & Beloborodov (2000). In particular, they show that the flow streamlines collide in the equatorial plane (which is the symmetry plane of the problem) and form a collision plate of radius r_d. The accretion then proceeds through the disc. Beloborodov & Illarionov (2000) have constructed a model of accretion through such a small-scale disc. Since the disc may form at $\sim r_g$, the relativistic effects cannot be neglected. Beloborodov & Illarionov (2000) studied accretion onto a Schwarzschild (nonrotating) black hole.

In this thesis, the effects of black hole rotation on the flow pattern are investigated. The black hole spin strongly affects the geometry of the space-time around the black hole. As a result, the radius of the disc should change. On the other hand, the radius of a rotating (Kerr) hole also depends on the spin. Therefore, the condition for disc formation will change as compared with the case of a nonrotating black hole. This effect will be studied here as well as other effects specific for Kerr holes, such as the effect of azimuthal "dragging" of the flow.

We will deal with relativistic free fall in the Kerr space-time. In the next section, we briefly review the basics of relativity, and the space-time geometry around nonrotating and rotating black holes.

4 Theory of relativity

Einstein proved that absolute time is fiction. The flow of time depends on motion and on the gravitational field. In a gravitational field all processes slow down for an outside observer. The gravitational fields change the geometric properties of space.

4.1 Special Relativity

The postulates of special relativity are:

The laws of physics have the same form in all inertial systems.

The velocity of light in empty space is a universal constant, the same for all observers.

The concept of inertial frames is important in special relativity. It is a reference system in which a body that is not affected by forces remain at rest or in uniform motion. All inertial frames are related by the Lorentz transformations.

Geometrically, space-time is represented by a four-dimensional manifold ("surface"), each point in the manifold corresponding to an event in space-time. An event is something that takes place at a given point in space and at a given point in time. Using the standard coordinates (t, x, y, z) with respect to some inertial system S, we can parameterize space-time by introducing the space-time coordinates: $x^0{=}ct$, $x^1{=}x$, $x^2{=}y$, $x^3{=}z$. These four coordinates are components of the so called *four-vector*

$$x^\mu = (ct, x^i) = (ct, \mathbf{r}). \tag{8}$$

When working in space-time, we use Greek suffixes (μ, ν, etc.) which can take the values 0,1,2,3, while in the three-dimensional space we use Roman suffixes (i, j, etc.) and these range from 1,2,3. The distance between two neighboring points in three-dimensional Euclidean space is

$$ds^2 = (dx^1)^2 + (dx^2)^2 + (dx^3)^2 = \begin{pmatrix} dx^1 \\ dx^2 \\ dx^3 \end{pmatrix}^t \begin{pmatrix} 1 & 0 & 0 \\ 0 & 1 & 0 \\ 0 & 0 & 1 \end{pmatrix} \begin{pmatrix} dx^1 \\ dx^2 \\ dx^3 \end{pmatrix} = (d\mathbf{r})^t G (d\mathbf{r}).$$

The 3×3 matrix G is called the *metric tensor* in Euclidean space. A tensor is a mapping from a vector to another vector, or as above; from a vector to a scalar.

By introducing the *Einstein summation convention*, which states that an index that occurs twice is summed over, we can write the metric equation in a more compact way

$$ds^2 = \sum_{i,j=1}^{3} G_{ij} dx^i dx^j \equiv G_{ij} dx^i dx^j . \tag{9}$$

Analogously we define the interval (or distance) between two nearby events in space-time as

$$\begin{aligned} ds^2 &\equiv -c^2 dt^2 + dx^2 + dy^2 + dz^2 = \\ &= -(dx^0)^2 + (dx^1)^2 + (dx^2)^2 + (dx^3)^2 . \end{aligned} \tag{10}$$

The interval ds does not depend on which inertial frame is used to evaluate it, it is *invariant.* ds^2 can be either positive or negative:

$$\begin{aligned} ds^2 &> 0 \quad \text{space-like separation} \\ ds^2 &< 0 \quad \text{time-like separation} \\ ds^2 &= 0 \quad \text{light-like separation} \end{aligned}$$

We can write equation (10) as

$$ds^2 = \eta_{\mu\nu} dx^\mu dx^\nu , \tag{11}$$

where

$$\eta_{\mu\nu} = \begin{pmatrix} -1 & 0 & 0 & 0 \\ 0 & 1 & 0 & 0 \\ 0 & 0 & 1 & 0 \\ 0 & 0 & 0 & 1 \end{pmatrix} . \tag{12}$$

This is the *metric tensor* of space-time in special relativity, which completely describes space-time geometrically. It is sometimes called the Minkowski metric, and space-time with this metric is called Minkowski space.

Since ds is invariant we can choose to measure the time in the rest frame moving with a particle ($dx = dy = dz = 0$)

$$ds^2 = \eta_{\mu\nu} dx^\mu dx^\nu = \left(dx^{0'} \right)^2 \equiv c^2 d\tau^2 . \tag{13}$$

This defines τ, the *proper time* as the time measured by a clock following the particle. In Galilean space-time there is only an absolute distance dt between events, and the spatial distance is dependent of the observer. Therefore, no Galilean invariant metric involving all of dx, dy, dz and dt exists.

4.2 General Relativity

The theory of special relativity applies to all physical phenomena except gravitation. Einstein succeeded in generalizing the theory of special relativity so that it also provided the law of gravity. This he called the theory of general relativity. The theory of special relativity treats inertial frames, but sometimes we would like to treat noninertial frames, e.g., rotating frames or accelerating frames. In general relativity, all frames are allowed and in a sense equal. The cornerstones of the general theory of relativity are the so called principles of equivalence:

Weak equivalence principle: This principle states that gravitational mass and inertial mass are equal. To make this somewhat easier to understand, consider a woman in a rocket without windows. Let her perform two experiments: First the rocket stands on the ground and she drops, for example, a hamster[1], which falls to the floor with an acceleration, g. Now put the rocket out in space, far from other gravitating bodies. If the rocket now accelerates, with an acceleration g in the direction of the ceiling, and she repeats the experiment, the hamster falls to the floor with the same acceleration. In the absence of windows, she cannot tell the difference between the two experiments. Locally there is no distinction between gravity and an accelerating frame of reference. This is the weak equivalence principle.

Strong equivalence principle: Now if the woman is standing in a freely falling elevator and drops another hamster, she will find that it is not affected by any forces, just like it would be if she dropped it out in space, in absence of gravitational fields. This shows that in a freely falling system, the gravitational force can be transformed away locally. A reference system falling freely in a homogeneous gravitational field is equivalent to an inertial system: the results of all local experiments in freely falling frames are consistent with the special theory of relativity.

These are the postulates of the general theory of relativity, and they are responsible for the following results:

Time runs slower in the presence of a gravitational field.

A ray of light is bent when traversing a gravitational field.

Introduce a metric tensor $g_{\mu\nu}(x^0, x^1, x^2, x^3)$. The distance between nearby events is given by

$$ds^2 = g_{\mu\nu} dx^\mu dx^\nu. \tag{14}$$

[1]This is only a gedanken experiment, no animals were injured during the writing of this thesis.

In contrast to the metric of special relativity, we allow the metric tensor to vary from point to point. $g_{\mu\nu}$ is a tensor field, i.e., it associates a tensor with every position in space-time. Space-time is in general curved due to the presence of matter. The strong equivalence principle implies that we can find a coordinate transformation from an arbitrary reference system to a local inertial frame. Locally, the space-time of general relativity looks like the space-time of special relativity. In special relativity we have *global* Cartesian coordinate systems where $g_{\mu\nu} = \eta_{\mu\nu}$ *exactly*, whereas in general relativity we have only *local* Cartesian coordinate systems, where $g_{\mu\nu} = \eta_{\mu\nu}$ *approximately*. We distinguish the two by saying that the space-time of special relativity is flat, while that of general relativity is curved.

We can construct a coordinate system about any point P of general-relativistic space-time in which

$$\left(\frac{\partial g_{\mu\nu}}{\partial x^\sigma}\right)_P = 0, \tag{15}$$

and $g_{\mu\nu} \approx \eta_{\mu\nu}$ to the first order. If we restrict ourselves to small space-time regions around P, the coordinates will transform linearly. We denote space-time coordinates in a local inertial frame with primes

$$dx'^\rho = \frac{\partial x'^\rho}{\partial x^\mu} dx^\mu, \tag{16}$$

where x^μ are coordinates in an arbitrary reference system, e.g., an accelerating frame. In a local inertial frame, the invariant expression defining the proper time τ is given by

$$c^2 d\tau^2 \equiv \eta_{\mu\nu} dx'^\mu dx'^\nu, \tag{17}$$

whereas in our arbitrary reference system it takes the form

$$c^2 d\tau^2 \equiv g_{\mu\nu} dx^\mu dx^\nu. \tag{18}$$

¿From the relation

$$\eta_{\rho\sigma} dx'^\rho dx'^\sigma = \eta_{\rho\sigma} \frac{\partial x'^\rho}{\partial x^\mu} \frac{\partial x'^\sigma}{\partial x^\nu} dx^\mu dx^\nu, \tag{19}$$

one gets the transformation rule for the metric tensor,

$$g_{\mu\nu} = \eta_{\rho\sigma} \frac{\partial x'^\rho}{\partial x^\mu} \frac{\partial x'^\sigma}{\partial x^\nu}. \tag{20}$$

The metric tensor $g_{\mu\nu}$ relates the different coordinate systems to each other, and defines the connection between measurements of, e.g., distances and time intervals to the coordinate intervals. Once you know the metric tensor you can specify the properties of space-time, such as curvature and distances.

The equation of motion for a free particle in terms of the free fall coordinate x'^{μ} is

$$\frac{d^2x'^{\mu}}{d\tau^2} = 0. \tag{21}$$

Transforming this to an arbitrary set of coordinates x^{μ} gives

$$\frac{d^2x^{\mu}}{d\tau^2} + \Gamma^{\mu}_{\nu\sigma}\frac{dx^{\nu}}{d\tau}\frac{dx^{\sigma}}{d\tau} = 0, \tag{22}$$

where

$$\Gamma^{\mu}_{\nu\sigma} = \frac{\partial x^{\mu}}{\partial x'^{\rho}}\frac{\partial^2 x'^{\rho}}{\partial x^{\nu}\partial x^{\sigma}}. \tag{23}$$

Equation (22) is called the *geodesic equation*, and $\Gamma^{\mu}_{\nu\sigma}$ are the *metric connections* or the *Christoffel symbols*. $\Gamma^{\mu}_{\nu\sigma}$ can be expressed in terms of the derivatives of the metric coefficients:

$$\Gamma^{\mu}_{\nu\sigma} = \frac{1}{2}g^{\mu\delta}\left(\frac{\partial g_{\delta\nu}}{\partial x^{\sigma}} + \frac{\partial g_{\delta\sigma}}{\partial x^{\nu}} - \frac{\partial g_{\nu\sigma}}{\partial x^{\delta}}\right). \tag{24}$$

In a flat space-time, $g_{\nu\mu} = \eta_{\nu\mu}$ and

4.3 Schwarzschild holes

The Schwarzschild black hole is named after Karl Schwarzschild, who in 1916 derived the relativistic solution for the gravitational field surrounding a *nonrotating*, electrically neutral sphere. To describe the space-time outside such a sphere one needs to develop the metric that tells us how the space-time is curved. Since we are dealing with spherical symmetry, it is convenient to use spherical coordinates (r, θ, ϕ). The Schwarzschild metric is given by the following expression:

$$ds^2 = -\left(1 - \frac{r_g}{r}\right)c^2dt^2 + \left(1 - \frac{r_g}{r}\right)^{-1}dr^2 + r^2d\theta^2 + r^2\sin^2\theta d\phi^2, \tag{25}$$

where r_g is the *Schwarzschild radius*,

$$r_g \equiv \frac{2GM}{c^2}, \tag{26}$$

M is the mass of the black hole, c is the speed of light.

At large distances, space-time is essentially flat. However, the behavior of space and time at $r = r_g$ is remarkable. For a photon traveling radially inwards, $d\theta = d\phi = 0$, and according to equation (25), $dr/dt = c(1 - r_g/r)$. Here it is taken into account that $ds^2 = 0$ for any photon. At $r \gg r_g$, $dr/dt \simeq c$ as expected in a flat space-time. However, at $r = r_g$, $dr/dt = 0$.

Time has slowed to a complete stop, as measured from our vantage point at rest a large distance away. ¿From our viewpoint, nothing ever happens at the Schwarzschild radius, because light is frozen in time at the Schwarzschild radius. The spherical surface at r_g acts as a barrier and prevents us from receiving any information from within. For this reason, a star that has collapsed down within the Schwarzschild radius is called a black hole. It is enclosed by the *event horizon*, the spherical surface at r_g. The Schwarzschild coordinates (25) behaves badly near $r = r_g$; there $g_{tt} = -(1 - r_g/r)$ becomes zero, and $g_{rr} = (1 - r_g/r)^{-1}$ becomes infinite. But this is due to a strange behavior of the coordinate system, rather than of the space-time geometry itself. The real singularity is at the center, a point of zero volume and infinite density where all of the black hole's mass is located. Space-time is infinitely curved at the singularity.

The Schwarzschild metric is a vacuum solution of Einstein's field equations, it is valid only in the empty space outside the object. The mathematical form of the metric is different in the object's interior, and will not be discussed here. Note that the event horizon is a mathematical surface and need not coincide with any physical surface. Although the interior of a black hole, inside the event horizon, is a region that is forever hidden from us on the outside, its properties may still be calculated.

To investigate the properties of the event horizon we let a very brave, and suicidal explorer fall in from far away towards the black hole, and we let her fall freely and radially into the event horizon. As she approaches the event horizon she notices no slowing of time, instead her proper time continues normally, and she encounters no frozen stellar matter since it has fallen through long ago. At $r = r_g$ there is a reversal of the roles of t and r as time-like and space-like coordinates. This means that the explorer has the option to turn on her jets and escape from the black hole whenever $r > r_g$, but inside the event horizon, $r < r_g$, she cannot escape. There the further decrease in r represents the passage of time, and therefore it is impossible to remain at rest. Within the event horizon of a nonrotating black hole, all worldlines converge at the singularity. Even photons are pulled in towards the center. This means that the explorer never has an opportunity to glimpse the singularity because no photons can reach her from there. She can, however, see the light that falls in behind her from events in the outside universe.

4.4 Kerr holes

Most of the astrophysical objects rotate, so we expect most black holes formed by gravitational collapse to be rotating. The Kerr black hole is rotating, and it is axially symmetric but not spherically symmetric. This solution of Einstein's equations, discovered in 1963 by R. Kerr (1963), was not at first recognized to be a black hole solution.

The most general stationary black hole metric, with parameters mass M, angular momentum J, and electric charge Q, is called the *Kerr-Newman metric.* A Kerr hole is the special case when $Q = 0$. Black holes in nature are expected to have $Q = 0$, since matter on a macroscopic scale is neutral. Written in the (t, r, θ, ϕ) coordinates of Boyer and Lindquist (1967), which is a generalization of the Schwarzschild coordinates, the Kerr metric has the form:

$$\begin{aligned} ds^2 = & - \left(1 - \frac{r_g r}{\rho^2}\right) c^2 dt^2 - \frac{2acr_g r \sin^2\theta}{\rho^2} dt d\phi + \frac{\rho^2}{\Delta} dr^2 + \\ & + \rho^2 d\theta^2 + \left(r^2 + a^2 + \frac{r_g r a^2 \sin^2\theta}{\rho^2}\right) \sin^2\theta d\phi^2. \end{aligned} \tag{27}$$

M is the mass of the black hole, and a is its specific angular momentum divided by c. The black hole is rotating in the ϕ direction, and

$$a \equiv \frac{J}{Mc}, \quad \Delta \equiv r^2 - r_g r + a^2, \quad \rho^2 \equiv r^2 + a^2 \cos^2\theta. \tag{28}$$

In textbooks one often use the so-called geometrical units, a system of units in which $c = G = 1$. In these units, the Schwarzschild radius is $r_g = 2M$. M is thus measured in cm. Here, I will not use the geometrical unit system, but the CGS system.

There is an off-diagonal term in the metric, in contrast to the Schwarzschild metric:

$$g_{t\phi} = \frac{acr_g r \sin^2\theta}{\rho^2}. \tag{29}$$

When setting $a = 0$ in equation (27) we get the Schwarzschild metric.

The component g_{tt} in the metric (27), which determines the rate of flow of time, vanishes at:

$$\rho^2 - r_g r = r^2 + a^2 \cos^2\theta - r_g r = 0,$$

or at $r = r_1$, where r_1 is given by

$$r_1 = \frac{r_g}{2} + \sqrt{\left(\frac{r_g}{2}\right)^2 - a^2 \cos^2\theta}. \tag{30}$$

The boundary $r_1(\theta)$ is called the *static limit* (see figure 5). No material bodies can be at rest within the surface $r = r_1(\theta)$. The reason for this is the same as in the Schwarzschild field at $r = r_g$. Namely, the world line of the observer ceases to be time-like, as indicated by the reversal of sign of g_{tt} at $r < r_1$. But an essential difference in comparison with the Schwarzschild field must be emphasized, because there are some additional features caused

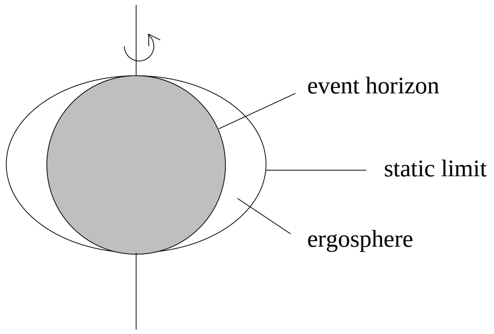

Figure 5: Near a rotating black hole, frame dragging is so severe that there is a nonspherical region outside the event horizon called the *ergosphere* where any particle must move in the same direction that the black hole rotates. The outer boundary of the ergosphere is called the *static limit*, so named because once inside this boundary a particle cannot possibly remain at rest there (i.e., be static) relative to the distant stars.

by the rotation. As a massive object spins, it induces a rotation in the surrounding space-time, a phenomenon known as *frame dragging*. If $r < r_1$, all bodies are unavoidably dragged into rotation, although r_1 is not the event horizon because a body may escape from this region. In the metric (27), the event horizon lies at $\Delta = 0$, that is, at $r = r_+$, where

$$r_+ = \frac{r_g}{2} + \sqrt{\left(\frac{r_g}{2}\right)^2 - a^2}. \tag{31}$$

For a rotating black hole, the Boyer-Lindquist coordinates are singular at the horizon. As in the Schwarzschild case, it requires an infinite time t (measured by an observer at rest far away from the black hole), for any particle or photon to fall through the event horizon. The dragging of inertial frames forces particles and photons near the horizon to orbit the black hole with $d\phi/dt > 0$. Consequently, for a particle falling through the horizon we have that $t \to \infty$ and also $\phi \to \infty$, an infinite twisting of worldlines around the horizon.

The region between the event horizon r_+ and the static limit r_1 is called the *ergosphere*. Space-time within the ergosphere is rotating so rapidly that a particle would have to travel faster than the speed of light to remain at the same angular coordinate (e.g. at the same value of ϕ in the coordinate system used by a distant observer). When $a = 0$, the static limit and the event horizon coincide, there is no dragging of inertial frames; there is no ergosphere.

There is an upper limit of a for a black hole to form, namely

$$\left(\frac{r_g}{2}\right)^2 \geq Q^2 + a^2.$$

If the black hole spins so fast that this constraint is violated, the centrifugal forces, will exceed the gravitational forces and halt the collapse. For a Kerr hole where $Q = 0$, this implies that the spin of the black hole must be $0 \leq a \leq r_g/2$. A black hole with $a = r_g/2$ is called an *extreme Kerr hole*. The event horizon for an extreme Kerr hole is situated at $r_+ = r_g/2$.

5 Method of calculations

The streamlines are symmetric with respect to the equatorial plane (the plane of the binary), and a streamline with angular momentum $l > l_{\rm min}$ will collide with the symmetric streamline coming from the other side of the equator. The trajectories of the streamlines are nearly parabolic. We will now derive an expression for the collision radius, for the Newtonian, Schwarzschild and Kerr cases.

5.1 Newtonian approximation

We start with the nonrelativistic Newtonian case. Assume that we have a point mass, with mass M, located at $x = 0$, $y = 0$, $z = 0$. A particle with velocity, v, and angular momentum per unit mass, l, comes in at an angle θ with respect to the z-axis (see figure 6). Very far away from the point mass we have that $\theta = \theta_\infty$, where the label "∞" corresponds to distances $r \gg r_g$. A particle coming from θ_∞ will cross the equator when $\theta = \pi/2$. The angular momentum per unit mass is

$$\mathbf{l} = \mathbf{r} \times \mathbf{v}.$$

In spherical coordinates (r, θ, ϕ), its components are

$$\begin{aligned} l_r &= 0, && (32) \\ l_\theta &= -r v_\phi, && (33) \\ l_\phi &= r v_\theta, && (34) \end{aligned}$$

and in Cartesian coordinates

$$\begin{aligned} l_x &= -r v_\phi \cos\theta \cos\phi - r v_\theta \sin\phi, && (35) \\ l_y &= -r v_\phi \cos\theta \sin\phi + r v_\theta \cos\phi, && (36) \\ l_z &= r v_\phi \sin\theta. && (37) \end{aligned}$$

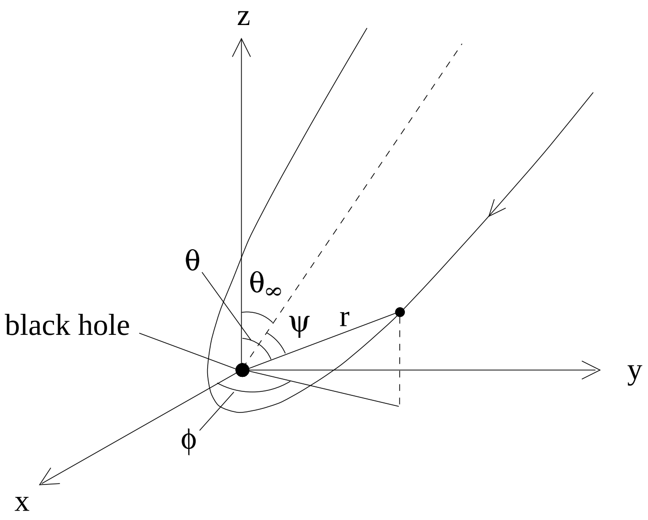

Figure 6: Particle orbit.

¿From equation (37) we get the ϕ-component of the velocity

$$v_\phi = \frac{l_z}{r \sin\theta}. \tag{38}$$

Using the relation between the angular momentum and its projection onto the z-axis

$$l_z = l \sin\theta_\infty,$$

and equations (32)-(34)

$$l^2 = l_r^2 + l_\theta^2 + l_\phi^2 = r^2 \left(v_\theta^2 + v_\phi^2 \right),$$

we get the θ-component of the velocity

$$v_\theta = \frac{l_z}{r} \sqrt{\frac{1}{\sin^2\theta_\infty} - \frac{1}{\sin^2\theta}}. \tag{39}$$

For a parabolic orbit, the total energy per unit mass is

$$E = \frac{v^2}{2} - \frac{GM}{r} = 0 \qquad \Longleftrightarrow \qquad v_r^2 + v_\theta^2 + v_\phi^2 = \frac{2GM}{r}, \tag{40}$$

and from this last equation we now get the r-component of the velocity, which is negative since the particle travels from ∞ to r,

$$v_r = -\sqrt{\frac{2GM}{r} - \frac{l_z^2}{r^2 \sin^2\theta_\infty}}. \tag{41}$$

Since $v_r = dr/dt$ and $v_\theta = r d\theta/dt$, we get a relation between r and θ

$$\frac{dr}{d\theta} = -\sqrt{\left(\frac{2GMr^3}{l_z^2} - \frac{r^2}{\sin^2\theta_\infty}\right)\left(\frac{\sin^2\theta_\infty \sin^2\theta}{\sin^2\theta - \sin^2\theta_\infty}\right)}. \tag{42}$$

Separate r and θ and integrate

$$\int_\theta^{\theta_\infty} \frac{\sin\theta_\infty \sin\theta}{\sqrt{\sin^2\theta - \sin^2\theta_\infty}} d\theta = \int_r^\infty \frac{dr}{\sqrt{\frac{2GMr^3}{l_z^2} - \frac{r^2}{\sin^2\theta_\infty}}},$$

which gives

$$\sin\theta_\infty \left[\arccos\left(\frac{\cos\theta}{\cos\theta_\infty}\right)\right] = \int_r^\infty \frac{dr}{\sqrt{\frac{2GMr^3}{l_z^2} - \frac{r^2}{\sin^2\theta_\infty}}},$$

which finally results in

$$\frac{\cos\theta}{\cos\theta_\infty} = \cos\left(\int_r^\infty \frac{dr}{\sqrt{\frac{2GMr^3}{l^2} - r^2}}\right) = \cos\Psi, \tag{43}$$

where

$$\Psi(r) = \int_r^\infty \frac{l dr}{\sqrt{r_g c^2 r^3 - l^2 r^2}}. \tag{44}$$

This integral can be solved analytically

$$\Psi(r) = 2\arccos\sqrt{1 - \frac{l^2}{2GMr}},$$

or,

$$\cos\Psi = 1 - \frac{l^2}{GMr}. \tag{45}$$

When $\Psi = \pi/2$ we have that

$$r = \frac{l^2}{GM}, \tag{46}$$

and this is the radius of collision in the equatorial plane. This radius can also be found from geometrical considerations, using the equation of a parabola in polar coordinates (r, Ψ)

$$r = \frac{A}{1 - \cos\Psi},$$

where A is a constant. By using the fact that energy is conserved and considering the case $\Psi = \pi$, we find that $A = l^2/GM$. The trajectory crosses the equatorial plane at $\Psi = \pi/2$ (see figure 6), hence the collision radius equals A, which gives the same expression as in equation (45).

5.2 Exact general relativistic calculation

The Newtonian approximation is valid when $r \gg r_g$. If the collision occurs close to the horizon, the general relativistic effects should be taken into account. The trajectory of a freely falling particle is described by the geodesic equation (22), which is a second order equation. The first integrals of this equation can be easily found for the Schwarzschild metric, which gives explicit expressions for the particle four-velocity, $u^\mu = dx^\mu/d\lambda$, (see Misner et al. 1973). A particle traveling along a parabolic trajectory, has specific orbital energy $E = c^2$, and

$$\frac{dt}{d\lambda} = \left(1 - \frac{r_g}{r}\right)^{-1}, \tag{47}$$

$$\frac{dr}{d\lambda} = -\sqrt{\frac{r_g c^2}{r} - \frac{l^2}{r^2}\left(1 - \frac{r_g}{r}\right)}, \tag{48}$$

$$\frac{d\theta}{d\lambda} = \frac{l_z}{r^2}\sqrt{\cot^2\theta_\infty - \cot^2\theta}, \tag{49}$$

$$\frac{d\phi}{d\lambda} = \frac{l_z}{r^2 \sin^2\theta}. \tag{50}$$

where λ is the proper time of a free-falling particle. Only the radial velocity is affected by the relativistic effects, and dividing u^r with u^θ, as we did above in the Newtonian case, we get

$$\frac{\cos\theta}{\cos\theta_\infty} = \cos\Psi,$$

where

$$\Psi(r) = \int_r^\infty \frac{l dr}{\sqrt{r_g c^2 r^3 - l^2 r^2 \left(1 - \frac{r_g}{r}\right)}}. \tag{51}$$

This differs from the Newtonian expression (44) only by a factor of $(1 - r_g/r)$. Setting $\Psi = \pi/2$, we get the the equation for the collision radius as a function of l outside a Schwarzschild hole

$$\int_r^\infty \frac{l dr}{\sqrt{r_g c^2 r^3 - l^2 r^2 \left(1 - \frac{r_g}{r}\right)}} = \frac{\pi}{2}. \tag{52}$$

When $r \gg r_g$, $1 - r_g/r \approx 1$, and we obtain the Newtonian solution of equation (44).

For a particle traveling along a parabolic trajectory, in the gravitational field of a rotating black hole, the integrals of motion are:

$$\rho^2 \frac{dt}{d\lambda} = -a\left(a\sin^2\theta - \frac{l_z}{c}\right) + \frac{r^2+a^2}{\Delta}\left(r^2+a^2-\frac{l_z}{c}a\right), \tag{53}$$

$$\rho^2 \frac{dr}{d\lambda} = c\sqrt{\left(r^2+a^2-\frac{l_z}{c}a\right)^2 - \Delta\left[r^2+\left(\frac{l_z}{c}-a\right)^2+Q^*\right]}, \tag{54}$$

$$\rho^2 \frac{d\theta}{d\lambda} = c\sqrt{Q^* - \frac{l^2}{c^2}\cos^2\theta}, \tag{55}$$

$$\rho^2 \frac{d\phi}{d\lambda} = c\left[-\left(a - \frac{l_z}{c\sin^2\theta}\right) + \frac{a}{\Delta}\left(r^2+a^2-\frac{l_z}{c}a\right)\right]. \tag{56}$$

Here l_z is the constant projection of the angular momentum of a particle on the rotation axis of the black hole, and Q^* is the integral of motion found by Carter (1968):

$$Q^* = \frac{l^2}{c^2}\cos^2\theta_\infty.$$

Following the same procedure as above, we get the equation for the collision radius in the Kerr case:

$$\int_r^\infty \frac{l\,dr}{c\sqrt{\left(r^2+a^2-\frac{l_z}{c}a\right)^2 - \Delta\left[r^2+\left(\frac{l_z}{c}-a\right)^2+Q^*\right]}} = \frac{\pi}{2}. \tag{57}$$

If we put $a = 0$, we get the same expression as in the Schwarzschild case.

5.3 Numerical calculation

To calculate at what distance, r, from the black hole a streamline reaches the equatorial plane, we must solve the integral in equation (57). This can be done by guessing a value of r, integrate, and hope that $\Psi(r) = \pi/2$. Doing this more methodically, I used a program called MatLab to do the guessing for me.

The code is simple, consisting mainly of three parts. First it divides the integration interval into smaller intervals of equal length, h. The integral is then evaluated for each smaller interval with the trapezoidal method. The intervals are summed up as we go along, and when the sum exceeds $\pi/2$ we repeat the procedure, but with a smaller value of h. In this way we can achieve a certain accuracy.

The integration limits are from r to infinity, and so the first interval will be from $r_\infty = r_0$ to a radius for which $\Psi > \pi/2$. Since the integrand is small and increases slowly for large r, a sufficiently large value of r_∞ will not radically change the value of the integral.

As the minimum radius, we can choose the radius which we know will give $\Psi > \pi/2$, the so-called turning point, $r_{\rm tp}$, for which $dr_{\rm tp}/dt = 0$. It is the point on the trajectory where a streamline is at the closest distance to the black hole. It is better to use a logarithmic step, since it is important to have a small step length at small r. The code is organized as follows:

1. $\ln r_0 - \ln r_{\rm tp}$ is divided into N intervals of equal length h. The first interval, I_1, will be from $\ln r_0$ to $\ln r_1$, where $\ln r_1 = \ln r_0 - h$, $\ln r_0 > \ln r_1$, and so on.

2. We denote the integral over the first interval as Ψ_1. If $\Psi_1 < \pi/2$, we take the next interval from $\ln r_1$ to $\ln r_2 = \ln r_1 - h$ and calculate the integral Ψ_2 for this interval. If $(\Psi_1 + \Psi_2) < \pi/2$ this procedure is repeated, until the sum $\Psi_{\rm tot} > \pi/2$ at some radius $\ln r_i$.

3. Now we start from the beginning again, only this time we choose a new N, say $N' = 5N$. The new intervals will thus be smaller, $h' = (\ln r_0 - \ln r_{\rm tp})/N'$. The same procedure as above is now repeated, and so this proceeds, until we are within a given accuracy.

6 Results

6.1 The collision radius and $l_{\rm min}$

I now calculate the collision radius of two symmetric streamlines with angular momentum l. The streamlines start at polar angles θ_∞ and $\pi - \theta_\infty$, and the collision occurs when they reach the equatorial plane, $\theta = \pi/2$ (see figure 6). The collision occurs outside the event horizon if the angular momentum exceeds the value $l_{\rm min}$, such that $r(l_{\rm min}(\theta_\infty)) = r_+$.

In the Newtonian approximation, $l_{\rm min} = r_g c/\sqrt{2} \approx 0.707 r_g c$, and does not depend on θ_∞. In the Schwarzschild case, $r_+ = r_g$, and from the numerical calculation of equation (57), setting $a = 0$, we find that $l_{\rm min} \approx 0.754 r_g c$ in agreement with Beloborodov & Illarionov (2000). Again, $l_{\rm min}$ does not depend on θ_∞. Plotting the difference between the Newtonian approximation and the exact relativistic calculation for a nonrotating hole, we see that the collision radius differs by $\sim 14\%$ at $r = r_g$ (figure 7).

In the case of a Kerr black hole, the collision radius depends not only on l, but also on θ_∞, and this is illustrated in figure 8. Hence, $l_{\rm min}$ is a function of θ_∞ (and since the spin changes the size of the black hole, it is also a function of a). The figures 9 and 10 show how the minimum angular momentum, $l_{\rm min}$ changes with θ_∞ and a, respectively. In the extreme Kerr case, which is when the black hole is maximally rotating ($a = r_g/2$), we have that $r_+ = r_g/2$. Then, the difference between the Newtonian approximation and the exact relativistic calculation is at most $\sim 35\%$ at the poles ($\theta_\infty \approx 0, \pi$), and decreases as $\theta_\infty \to \pi/2$ (see figure 11). For $\theta_\infty = \pi/2$ the Kerr solution does

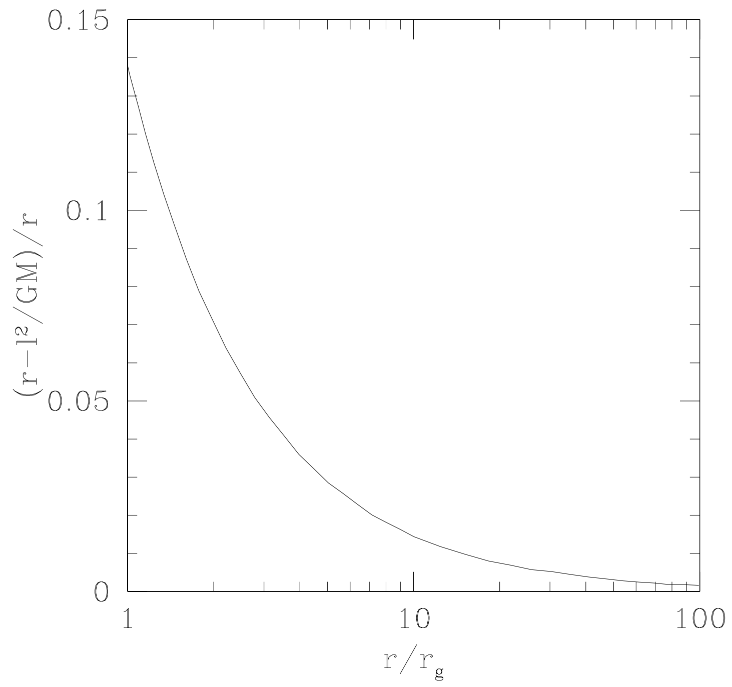

Figure 7: The error of the Newtonian approximation, $r = l^2/GM$, for the collision radius, $r(l)$, near a nonrotating black hole. The collision radius is given by equation (52).

almost not differ from the Newtonian solution at all. Thus, for a rotating black hole, the trajectory of the gas flow is altered more severely by the relativistic effects at the poles.

Letting a be negative, i.e. the black hole is rotating in the opposite direction, we now calculate the collision radius again. $r(l)$ is clearly affected when changing the direction of the spin (see figure 12), especially the streamlines passing close to the equatorial plane. This is so because they will, instead of continuing their trajectories around the black hole, be deflected towards the face of the black hole as a result of the frame dragging (see section 4.4, see also section 6.2 below). Streamlines that in the case of positive spin would collide just outside the event horizon, will instead be deflected into the black hole for a negative spin. Plotting the difference between the exact relativistic calculation (with $a = -r_g/2$), and the Newtonian approximation (see figure 13), we see that the difference is as large as $\sim 75\%$ at $\theta_\infty = \pi/2$, and it is small for flow along the poles ($\theta_\infty \approx 0, \pi$).

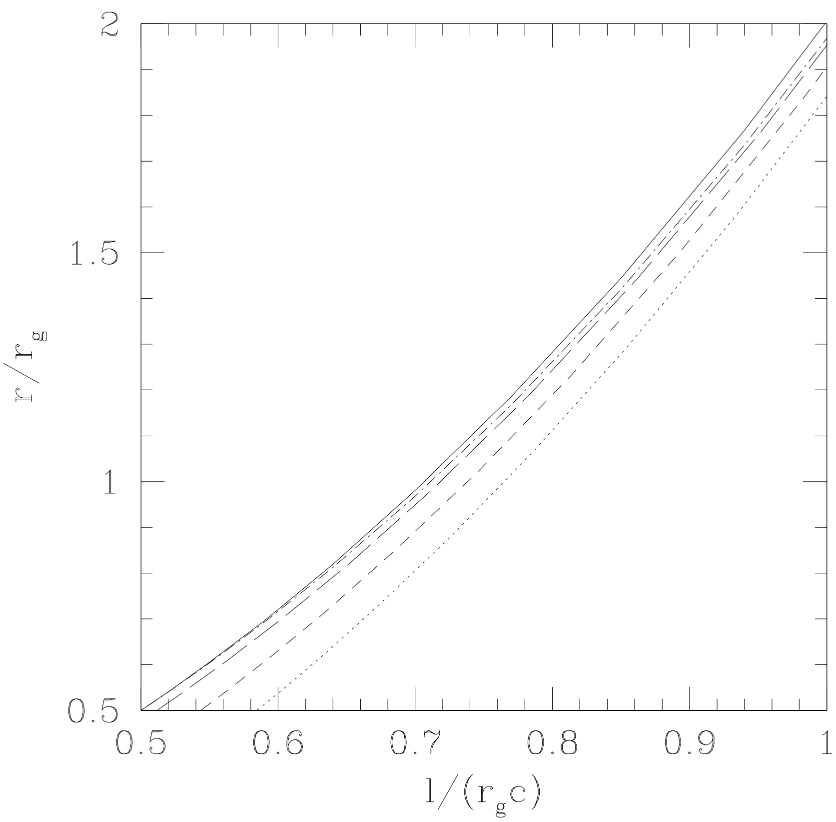

Figure 8: The calculated collision radius as a function of the angular momentum, in the case of extreme Kerr hole, $a = r_g/2$. $r(l)$ is here plotted for different values of θ_∞, $\theta_\infty = 0°$ (dotted line), 30° (short dash), 60° (long dash), 90° (dash dot) and the Newtonian solution (solid line). The collision radius is affected by the spin of the black hole, the trajectories coming in from the poles ($\theta_\infty = 0°$) are altered the most.

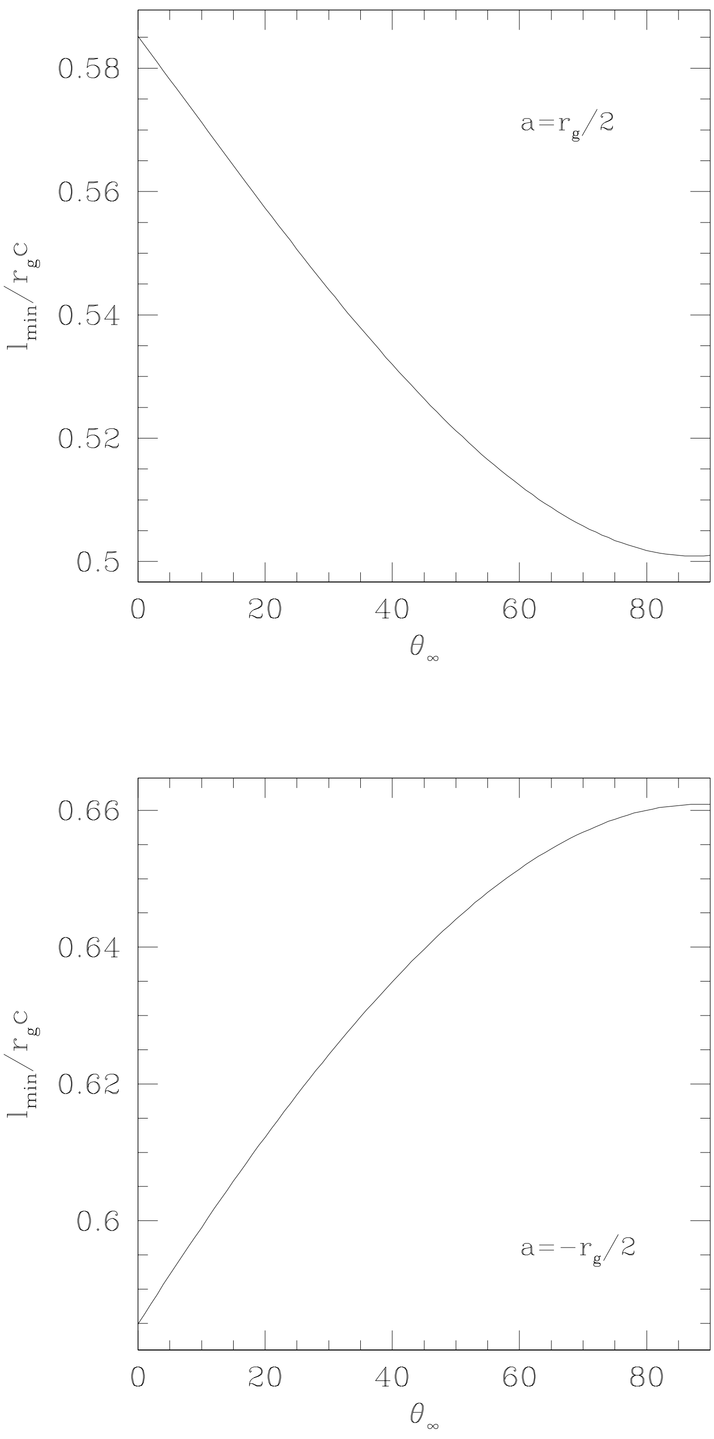

Figure 9: For an extreme Kerr hole, the minimum angular momentum a streamline can have for collision outside the event horizon, is $r(l_{\rm min}) = r_g/2$. Here $l_{\rm min}$ is plotted as a function of θ_∞, for $a = r_g/2$ and $a = -r_g/2$.

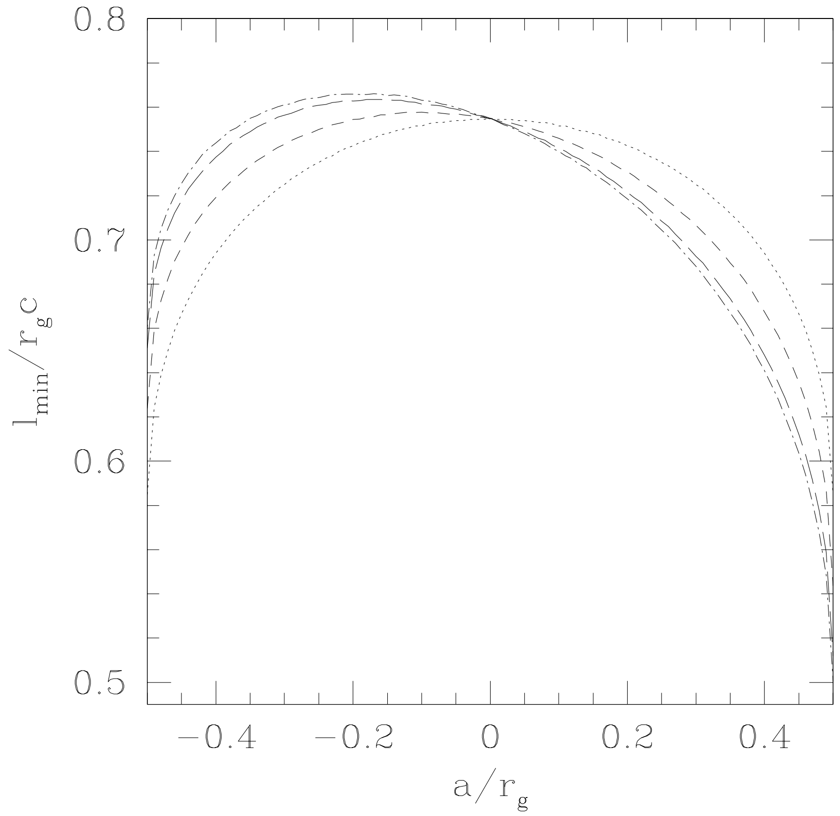

Figure 10: The minimum angular momentum, $l_{\min}$, as a function of the spin, a, of the black hole. $l_{\min}$ varies with θ_∞, here $\theta_\infty = 0°$ (dotted line), $30°$ (short dash), $60°$ (long dash) and $90°$ (dash dot).

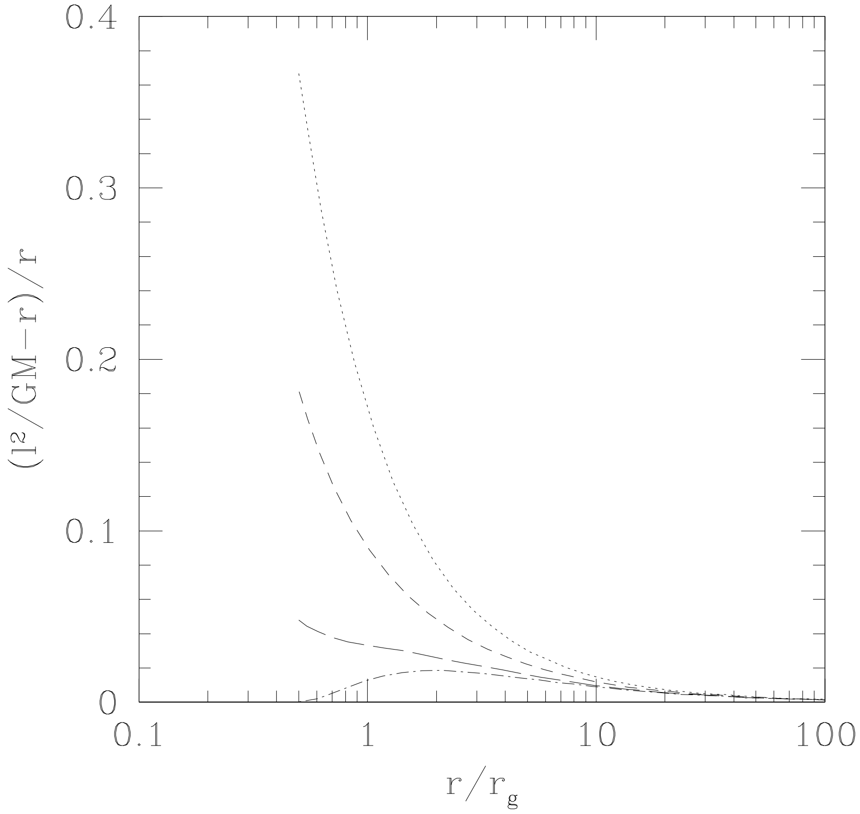

Figure 11: The error of the Newtonian approximation, $r = l^2/GM$, for the collision radius, $r(l)$, in the case of a rotating black hole. The collision radius, $r(l)$, is given by equation (57). It is plotted for $\theta_\infty = 0°$ (dotted line), 30° (short dash), 60° (long dash) and 90° (dash dot). Closer to the equatorial plane, the trajectories do not differ much from the Newtonian solution. One can say that the rotation of the black hole reduces the relativistic effects towards the equatorial plane, and the trajectories there can be described by the Newtonian approximation.

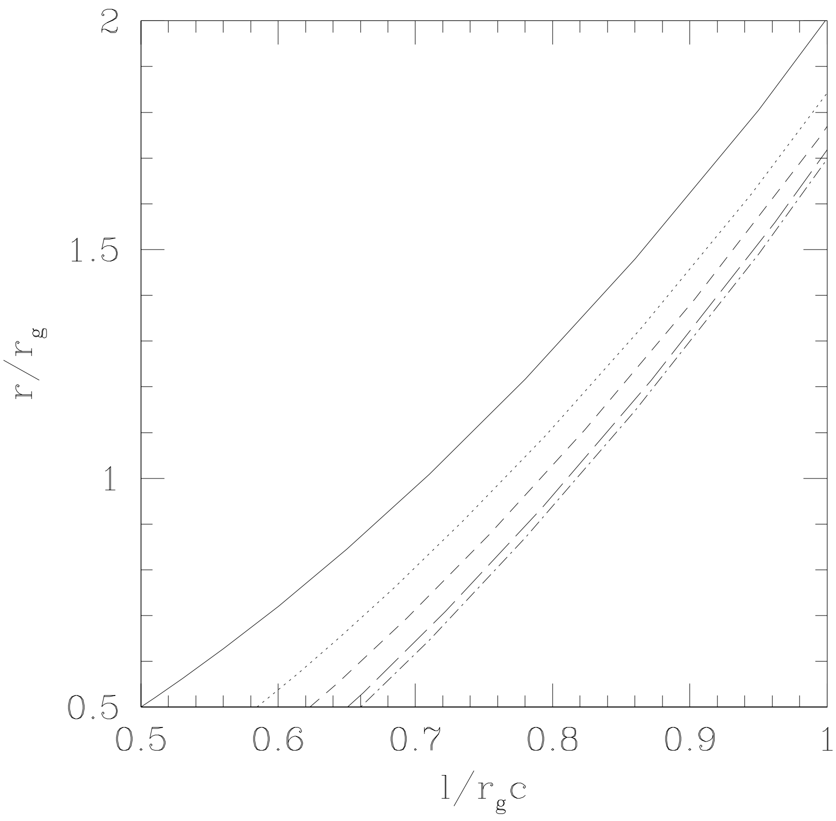

Figure 12: The collision radius, $r(l)$, for the opposite black hole spin $a = -r_g/2$. Along the poles ($\theta_\infty \approx 0, \pi$), the motion of a streamline is nearly perpendicular to the frame dragging, thus it will not be affected much by the change in direction of spin. At $\theta_\infty \approx \pi/2$ the streamlines encounter the opposite frame dragging, and therefore, they are more affected by the change in sign of spin. Here $\theta_\infty = 0°$ (dotted line), 30° (short dash), 60° (long dash), 90° (dash dot) and the Newtonian solution (solid line).

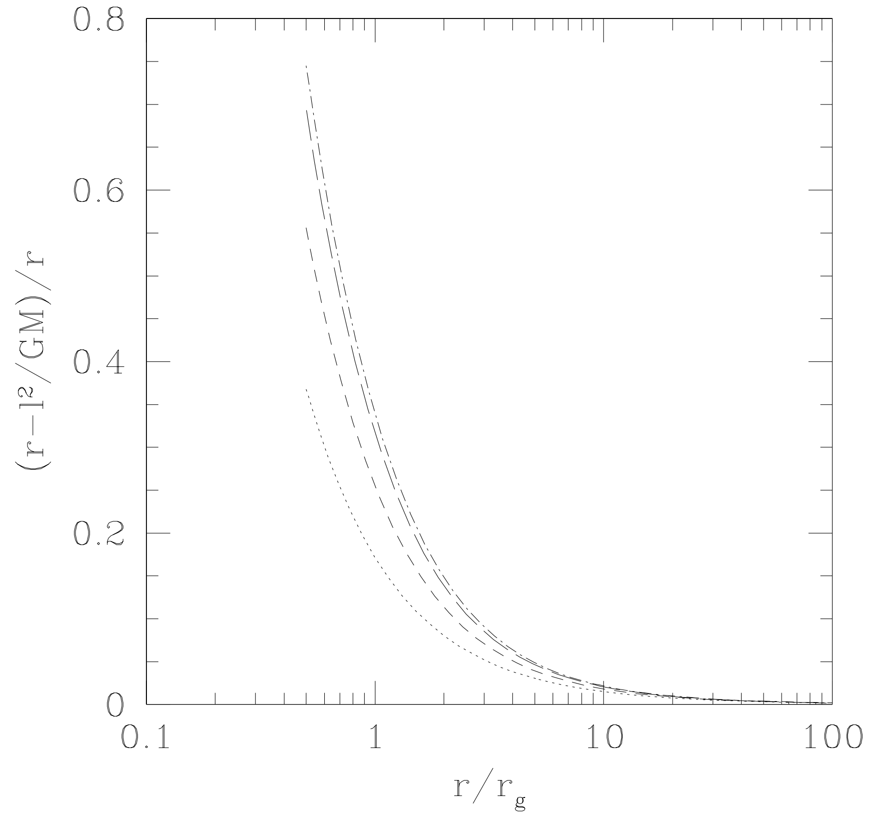

Figure 13: The error of the Newtonian approximation, $r = l^2/GM$, for $r(l)$ given by equation (57) in the case $a = -r_g/2$. The error is plotted for $\theta_\infty = 0°$ (dotted line), 30° (short dash), 60° (long dash) and 90° (dash dot).

6.2 The azimuthal angle of collision

Because of the rotation of the black hole, the trajectory of a streamline will not only be affected radially by the relativistic effects, but also in the ϕ-direction. In Newtonian gravity, streamlines will make a $\pi/2$ turn around the polar axis before reaching the equatorial plane, and this is also true for a streamline in the gravitational field of a nonrotating black hole, since the streamline is only affected in the radial direction. The rotation of the black hole causes space-time to rotate in the azimuthal direction, a phenomenon known as frame dragging (see section 4.4). The streamlines will of course be affected to a certain degree by this dragging, depending on how close to the event horizon they reach the equatorial plane. A streamline with large angular momentum, will collide further away from the black hole, and its trajectory will not be as affected by the dragging as a streamline with low angular momentum, which collides closer to the event horizon.

We can calculate how the rotation of the black hole affects the trajectory in the ϕ-direction by using the integrals of motion given in section 4.4. From equation (54) and equation (56), we get a relation between r and ϕ:

$$\phi - \phi_\infty = \int_r^\infty \frac{-\left(a - \frac{l_z}{c\sin^2\theta}\right) + \frac{a}{\Delta}\left(r^2 + a^2 - \frac{l_z}{c}a\right)}{\sqrt{\left(r^2 + a^2 - \frac{l_z}{c}a\right)^2 - \Delta\left[r^2 + \left(\frac{l_z}{c} - a\right)^2 + Q^*\right]}} dr. \qquad (58)$$

The collision radius will be affected by the rotation, depending on the value of θ_∞. The streamlines coming in at the poles will make a longer turn around the black hole before reaching the equatorial plane, as compared to the streamlines with a larger value of θ_∞. Figure 14 shows how $\phi - \phi_\infty$ changes with the angular momentum, l, for $a = r_g/2$ and different values of θ_∞.

When changing the spin to the opposite direction, $a < 0$, we get a somewhat different result. The streamlines coming in from the poles are unchanged, while the greater θ_∞, the more affected $\phi - \phi_\infty$ is by the rotation (see figure 15). This is a result of frame dragging which also modifies the collision radius, $r(l)$, in a way described in section 6.1.

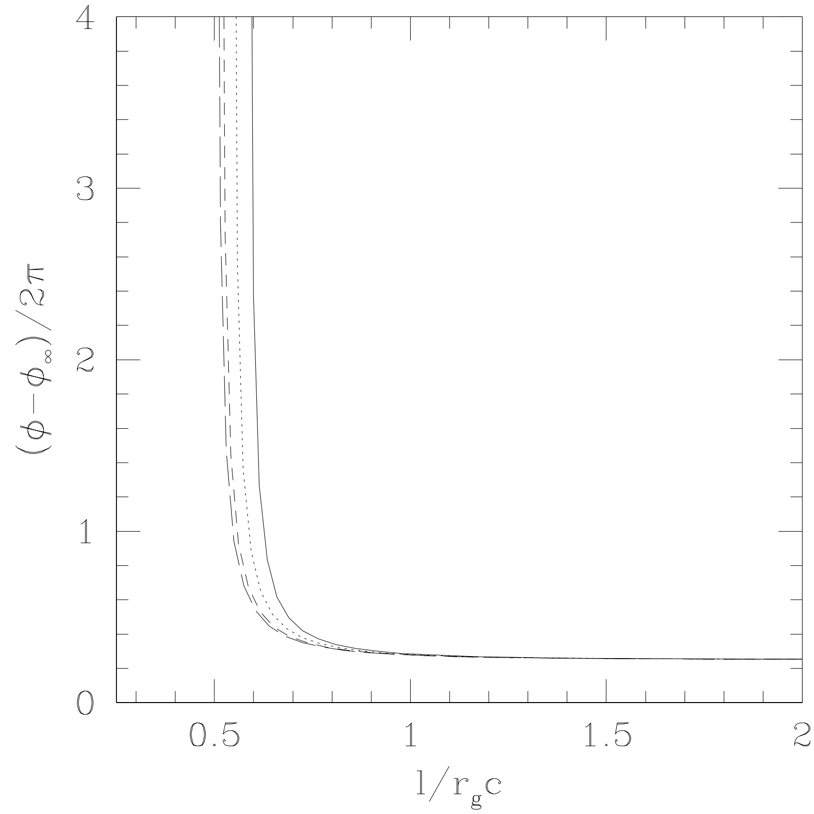

Figure 14: The azimuthal angle, $\phi - \phi_\infty$, when $a = r_g/2$, plotted for $\theta_\infty = 0°$ (dotted line), 30° (short dash), 60° (long dash) and 90° (dash dot). The y-axis is given as the number of turns a streamline executes, with respect to the black hole, before reaching the equatorial plane. $(\phi-\phi_\infty)/2\pi$ should be 1/4 at large distances, and here $(\phi - \phi_\infty)/2\pi = 1/4$ down to $l \sim r_g c$ corresponding to $r \sim 2r_g$.

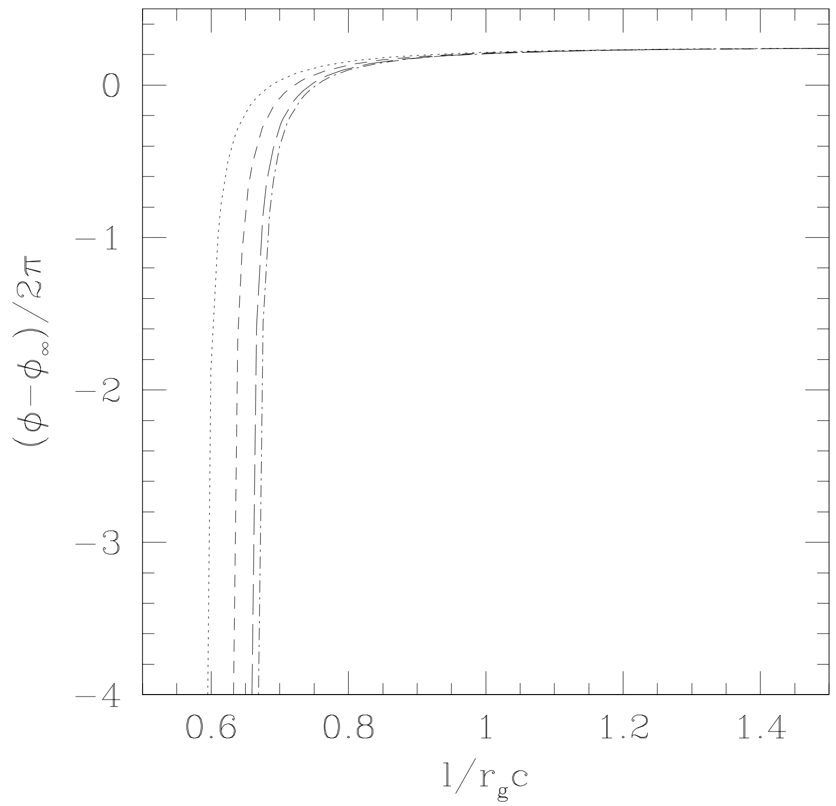

Figure 15: The azimuthal angle, $\phi - \phi_\infty$, when $a = -r_g/2$, plotted for $\theta_\infty = 0°$ (dotted line), $30°$ (short dash), $60°$ (long dash) and $90°$ (dash dot). The effects of the frame dragging can be seen here, manifesting themselves as "negative" turns around the black hole.

6.3 Accretion rate through the disc

The collision of the symmetric streamlines leads to the formation of a small-scale disc in the equatorial plane. Because of the low angular momentum of the streamlines, the disc can accrete fast, and thus viscosity can be neglected. For a theoretical treatment of such a fast inviscid disc, assuming a nonrotating black hole, see Beloborodov & Illarionov (2000).

It is rather complicated to calculate the structure of the disc and its energy release, and I do not attempt to fully solve this problem to the end. However, we can look at the effects of the spin on the accretion rate, $\dot{M}$, through the disc. At a radius r, $\dot{M}(r)$ equals the rate of matter absorbed by the disc at $r' > r$ (see Beloborodov & Illarionov 2000). We assume a uniform radial inflow from $r \sim r_{\mathrm{C}}$,

$$\frac{d\dot{M}}{d\Omega} = \frac{\dot{M}_{\mathrm{tot}}}{4\pi} = constant,$$

where (King 1995)

$$\dot{M}_{\mathrm{tot}} \sim \frac{r_{\mathrm{acc}}^2 \dot{M}_{\mathrm{w}}}{4d^2}. \tag{59}$$

We also assume rigid rotation at $r \ll r_g$,

$$l = l_0 \sin\theta_\infty,$$

where l_0 is the angular momentum of gas falling in with $\theta \to \pi/2$, it is the angular momentum that corresponds to the largest collision radius.

The gas that collides outside r will have an angular momentum $l' > l$, and will fall in through a solid angle $\Omega_{l'>l}$. The accretion rate through this solid angle equals:

$$\dot{M}(r) = \dot{M}(l' > l) = \dot{M}_{\mathrm{tot}} \cos\theta_\infty(l).$$

Since $\sin\theta_\infty = l/l_0$, the mass accretion rate at r becomes

$$\dot{M}(r) = \dot{M}_{\mathrm{tot}}\sqrt{1 - \left(\frac{l}{l_0}\right)^2} = \dot{M}_{\mathrm{tot}}\sqrt{1 - \frac{l_z}{l_0}}, \tag{60}$$

where $l_z = l \sin\theta_\infty$ is the z-component of the angular momentum at r.

In figure 16, we can see that there is a small difference in the mass accretion rate for the cases $a = r_g/2$, $a = -r_g/2$ and $a = 0$, and the Newtonian approximation. Thus the mass accretion rate in discs around rotating black holes can be approximated by

$$\dot{M}(r) \approx \dot{M}_{\mathrm{tot}}\sqrt{1 - \frac{r}{r_0}}. \tag{61}$$

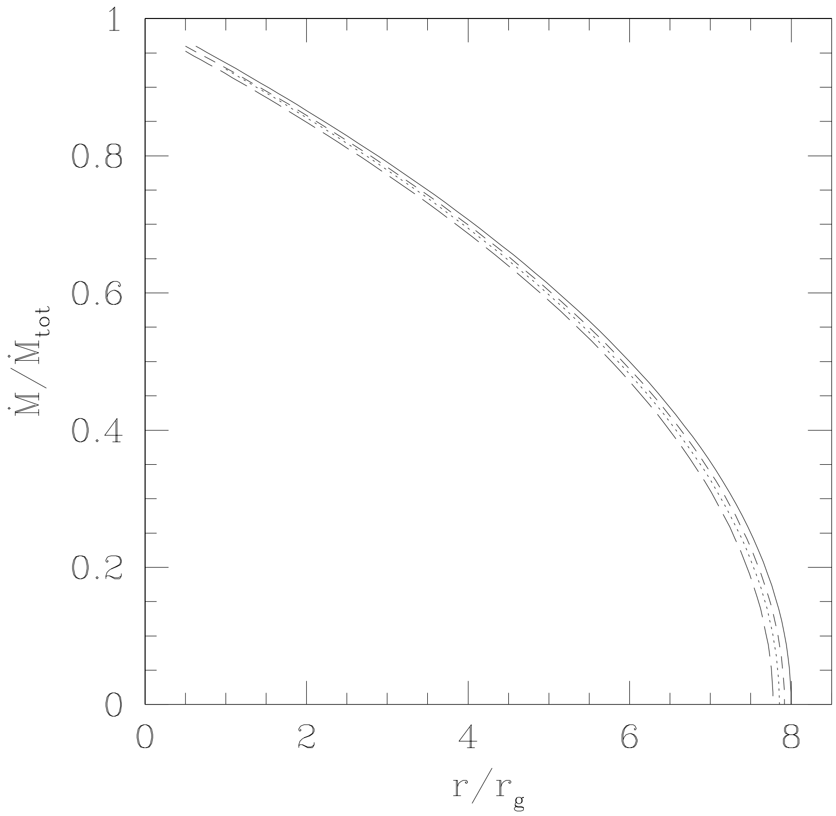

Figure 16: The mass accretion rate through the disc for $a = 0$ (dotted line), $a = r_g/2$ (short dash), $a = -r_g/2$ (long dash) and the Newtonian solution (solid line).

7 Conclusions

In spite of the theoretical approach of this thesis, the results do apply to real astrophysical objects. In fact, the black holes in massive X-ray binaries are very likely to rotate, and may have a large spin. The spin alters the collision radius differently, depending on whether the black hole is counter-rotating ($a < 0$) or co-rotating ($a > 0$) with the accretion flow. The azimuthal motion of the infalling gas is also altered because of the frame dragging induced by the rotation of the black hole.

Here are the main results for extreme Kerr black holes ($a = \pm r_g/2$):

(i) When $a = r_g/2$, the streamlines passing near the equatorial plane can be described by the Newtonian approximation $r = l^2/GM$, with a high accuracy. Along the poles, the streamlines differ from the Newtonian approximation by $\sim 35\%$.

(ii) When $a = -r_g/2$, the streamlines along the poles again differ from the Newtonian approximation by $\sim 35\%$. Thus the flow coming in from $\theta_\infty \approx 0, \pi$ is unaffected by the direction of the black hole spin. For the streamlines passing near the equatorial plane, the discrepancy is as much as $\sim 75\%$. Thus the collision radius is altered more by the relativistic effects in the case of a negative spin.

(iii) For both $a = r_g/2$ and $a = -r_g/2$, the azimuthal motion of a streamline coming in from along the poles is more affected by the rotation than that of a streamline passing near the equatorial plane.

(iv) The mass accretion rate through the disc was found to be nearly the same for $a = r_g/2$ and $a = -r_g/2$, and deviated little from the Newtonian approximation. $\dot{M}$ can thus be described by equation (61).

We did not calculate the energy release in the disc in this thesis, and this might be a subject of future studies.

Acknowledgements

I would like to thank Andrei Beloborodov for his excellent guidance and pedagogical skills, Erik B Johansson for lending me bits when unhorsed, Anders Gavler for feeding the bird, and all friends forgotten. I would also like to thank my mum and dad for, after much explaining, convincing me that we do not live inside the earth but upon its surface, thus giving me the insight that the "ceiling" was actually space.

References

[1] Beloborodov A. M. & Illarionov A. F., *Fast inviscid accretion discs around black holes*, (2000), MNRAS, submitted

[2] Bergström L. & Goobar A., *Cosmology and particle astrophysics*, (1999), John Wiley & Sons Ltd in association with Praxis Publishing Ltd

[3] Bondi H. & Hoyle F., (1944), *On the mechanism of accretion by stars*, MNRAS, 104, 273

[4] Boyer R. H. & Lindquist R. W., (1967), *Maximal analytic extension of the Kerr metric*, J. Math. Phys., 8, 265

[5] Carter B., (1968), *Global structure of the Kerr family of gravitational fields*, Phys. Rev., 174, 1559

[6] Charles P. A. & Seward D. S., *Exploring the X-ray Universe* (1995), Cambridge University Press, Cambridge

[7] Frank J., King A. & Raine D., *Accretion power in astrophysics*, (1985), Cambridge University Press, Cambridge

[8] Hunt R., (1971), *A fluid dynamical study of the accretion process*, MNRAS, 154, 141

[9] Igumenshchev I., Illarionov A. F. & Kompaneets D. A., *The outflowing regime of quasi-spherical accretion on to X-ray compact objects*, (1993), MNRAS, 260, 727

[10] Illarionov A. F. & Beloborodov A. M., *Wind-fed accretion: The appearance of emitting surfaces and caustics*, (2000), MNRAS, submitted

[11] Illarionov A. F. & Kompaneets D. A., *A spin-down mechanism for accreting neutron stars*, (1990), MNRAS, 247, 219

[12] Illarionov A. F. & Sunyaev R. A., (1975), *Why the number of galactic X-ray stars is so small?*, A& A, 39, 185

[13] Kerr R. P., (1963), *Gravitational field of a spinning mass as an example of algebraically special metrics*, Phys. Rev. Lett., 11, 237

[14] King A., *Accretion in close binaries*, (1995), in X-ray binaries, eds. W. H. G. Lewin, J. van Paradijs, and E. P. J. van den Heuvel, Cambridge University Press, Cambridge, p. 419

[15] McClintock J. & van Paradijs J., *Optical and ultraviolet observations of X-ray binaries*, (1995), in X-ray binaries, eds. W. H. G. Lewin, J. van Paradijs, and E. P. J. van den Heuvel, Cambridge University Press, Cambridge, p. 58

[16] Misner C. W., Thorne K. S. & Wheeler J. A, *Gravitation*, (1973), San Francisco: W.H. Freeman and Co.

[17] Rindler W., *Essential relativity: Special, general and cosmological* (1977), New York: Berlin: Springer-Vlg

[18] Shapiro S. L. & Lightman A. P., (1976), *Black holes in X-ray binaries - Marginal existence and rotation reversals of accretion disks*, ApJ, 204, 555

[19] Shapiro S. L. & Teukolsky S. A., *Black Holes, White Dwarfs and Neutron Stars, the Physics of Compact Objects*, (1983), John Wiley & Sons, Inc.

[20] Schutz B. F., *A First Course in General Relativity*, (1988), Cambridge University Press, Cambridge

[21] Tanaka Y. & Lewin W. H. G., (1995), *Black hole binaries* , in X-ray binaries, eds. W. H. G. Lewin, J. van Paradijs, and E. P. J. van den Heuvel, Cambridge University Press, Cambridge, p. 126